

Tracking fault-tolerant control based on model predictive control for human occupied vehicle in three-dimensional underwater workspace

Huapeng Zhang^b, Daqi Zhu^{a,*}, Chenxia Liu^{b,**}, Zhen Hu^c

^a The School of Mechanical Engineering, University of Shanghai for Science and Technology, Jungong Road 516, Shanghai, 200093, China

^b Shanghai Engineering Research Center of Intelligent Maritime Search & Rescue and Underwater Vehicles, Shanghai Maritime University, Haigang Avenue 1550, Shanghai, 201306, China

^c Underwater Engineering Institute, China Ship Scientific Research Center, Wuxi, 214082, China

ARTICLE INFO

Keywords:

Human occupied vehicle
Trajectory tracking
Quantum-behaved particle swarm optimization
Model predictive control
Adaptive control
Thruster fault-tolerant control

In this paper, for the human occupied vehicle (HOV) system, a cascaded dynamic tracking controller for thruster fault is proposed in three-dimensional underwater workspace. Firstly, the control strategies are used to reallocate the thruster forces based on quantum-behaved particle swarm optimization (QPSO) for thruster failure. Secondly, the kinematics controller based on QPSO-model predictive control (MPC) is designed to obtain the speed control signal. QPSO-MPC with speed constrained optimization is proposed to solve speed jump problem caused by thruster failure. Finally, the kinematics controller is used in conjunction with dynamics controller based on the adaptive control to achieve dynamic tracking control which can solve the driving saturation problem caused by thruster failure and tracking disturbance problem by unknown ocean current disturbance. Simulation results showed the proposed dynamic tracking control with fault-tolerant control could realize stable trajectory tracking for thruster failure without the driving saturation in three-dimensional ocean current environment.

1. Introduction

At present, the human occupied vehicle (HOV) is one of the frontiers and commanding heights of marine development. In the complicated ocean environment, once the HOV fault occurs, HOV cannot accomplish its mission and may produce threat to the life safety of aquanaut and scientist. Thruster failure as one of the most universal and significant fault sources (Zhang and Jiang, 2008; Valdes and Khorasani, 2010), once a failure occurs, the consequences will be very serious, so, fault-tolerant control of thruster is necessary. General Inverse (GI) is a universal algorithm for the redistribution of thruster force/moment after thruster failure (Omerdic and Roberts, 2004; Benosman and Lum, 2009). However, that algorithm can only get the solution space from the reachable command set, so it cannot handle the problem of control constraints. In order to deal with the situation that the available control inputs cannot be allocated. Two methods, the T-approximation (Truncation) and the S-approximation (Scaling) were proposed (Zhu et al., 2011). But these two approximation methods also exist errors of the magnitude and direction which cause by scaling or truncation so that the HOV cannot fully follow the reference trajectory. A chattering-free sliding-mode controller with the infinity-norm thrust allocation

fault-tolerant control was proposed for underwater vehicles and satisfied the saturation limits of each thruster (Soylu et al., 2008). Non-Linear Principal Component Analysis was used to address the problem of Fault Detection and Isolation on thrusters of an over-actuated AUV under on/off abrupt faults (Fabiani et al., 2016). The CNN was introduced to learn the mapping from the logged motion sequence to the status of the thruster to detect and isolate potential thruster failure (Han et al., 2020). However, the HOV dynamic trajectory tracking control problem with thruster faults in ocean current had little discuss.

Stable trajectory tracking in complex underwater environment is one of the most important properties of HOV (Yan et al., 2012, 2015). Any underwater activities will become very challenging because of the existence of ocean current. In the field of underwater vehicle control, some scholars had also made some breakthroughs to eliminate the influence of ocean current. In the presence of constant ocean current, adaptive neural network-based backstepping fault tolerant control was applied for underwater vehicles with thruster fault and realized the effective trajectory tracking of underwater vehicle under model uncertainty, ocean current, tether force and thruster failure (Wang et al., 2015). Controlled Lagrangian particle tracking was used to develop an adaptive learning algorithm that allows AUVs to learn their true motion in ocean

* Corresponding author.

** Corresponding author.

E-mail addresses: zdq367@aliyun.com (D. Zhu), 7000m@vip.sina.com (Z. Hu).

flow fields in real time (Cho et al., 2017). For the constrained control problem, some scholars also have made progress on it. For instance, considering thruster saturation, a fresh controller based on Lyapunov-model predictive control (MPC) method is developed, the thrust control law is positively correlated with position error to realize constraint control to improve trajectory tracking performance (Shen et al., 2018). For track tracking in the 2-D vertical plane, a method included an outer-loop guidance law, an inner-loop control law and a reference governor was proposed (Peng et al., 2019). Then, the research area extended to three-dimension (3-D) and constant ocean current environment (Gan et al., 2020a,b) was added.

Obviously, the constant ocean current is too ideal and simple and the discussion about the HOV fault-tolerant control of trajectory tracking had not been reported in time-varying ocean current. In this paper, the influence of both ocean current and thruster failure will be considered. MPC intends to solve the speed jump problem by applying speed constraints for HOV system (McCue, 2016; Fossen and Sagatun, 1991; Naeem et al., 2004). MPC is a based on the object model sophisticated control algorithm, there are three key points to apply MPC, including, prediction model, rolling optimization and feedback correction. Meanwhile, the ability of multivariate constraints is the biggest attraction of MPC. This ability stems from itself model-based prediction for system future dynamic behavior, and then the constraints will be applied to future inputs, outputs or state variables. In addition, for the MPC optimization process, that is not executed once offline, but repeatedly online which can compensate for uncertainties caused by model mismatch, distortion and interference. Considering the good quality of solution, robustness and global convergence, QPSO algorithm is used in the rolling optimization process. For HOV system, various speed constraints are included in the QPSO optimization process (Gao et al., 2016; Shen et al., 2017; Sun et al., 2004), these characteristics can play a great role to deal with the speed jump problem valid. Then it is extended to dynamics control. Adaptive control has been used in dynamic tracking control for many years. If the adaptive rate of parameters is appropriate, because the adaptive control has the ability to make the controller modify its own characteristics to adapt to the dynamic characteristics of targets and disturbances, it is robust and can effectively overcome tracking disturbances (Li and Zhu, 2018).

In this paper, a novel cascaded dynamic tracking controller with thruster failure is realized, which jointing kinematics controller based on QPSO-MPC, dynamics controller based on adaptive control and thruster fault-tolerant control could achieve stable trajectory tracking control and solve driving saturation problem caused by speed jump under thruster failure. The simulation results show that the proposed cascade dynamic tracking controller can fully achieve the anticipated target.

This paper is organized as follows. In section 2, the kinematics and dynamics model of HOV is established. Then the kinematics controller is designed by QPSO-MPC method and the adaptive control is used to devise the dynamics controllers. Finally, in order to estimate the unknown ocean current, an observer based on Adaptive-PI control was designed. In section 3, the thruster fault-tolerant control method is described. In section 4, trajectory tracking under thruster failure situation in ocean current environment simulations results are discussed. Finally, concluding is given in section 5.

2. Modeling of HOV and dynamic tracking controller

In this paper, take the Deep-sea Warrior HOV as the trajectory tracking control research object. When HOV is working underwater, the roll and pitch under 6-degrees of freedom (DOF) should be avoided. Therefore, the HOV model is decoupled and controlled in 4-DOF, namely, surge, sway, yaw and heave.

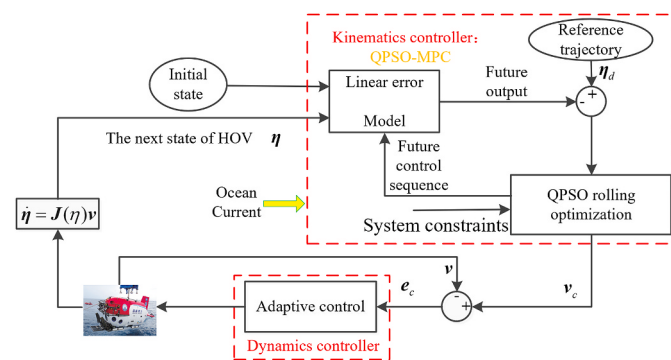


Fig. 1. The diagram of dynamic tracking control.

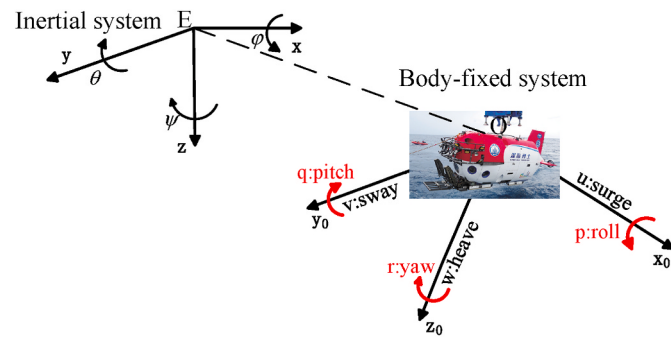


Fig. 2. HOV coordinate system.

The cascaded dynamic tracking controller of HOV is put forward to obtain thrusts. First, in the part of kinematics, the QPSO-MPC-based kinematics controller is made up linear error model, system constraints and the objective function solved by QPSO algorithm. Meanwhile, according to the speed synthesis method, the ocean current which obtained by ocean current observer was introduced into the kinematics controller. Then, union QPSO-MPC-based kinematics controller and adaptive-based dynamics controller to achieve dynamic tracking control. Among it, the controlling increment values obtained by kinematics controller will be employed as input to dynamics controller. Finally, the expected force/moment computed by dynamics controller are transmitted to fault-tolerant control part. And the propulsion system of Deep-sea Warrior HOV have been completed (Gan et al., 2020a,b). The HOV dynamic tracking control is shown in Fig. 1.

2.1. Kinematics modeling

The HOV system could be regarded as a control system with speed $v = [u \ v \ w \ r]^T$ and the state $\eta = [x \ y \ z \ \psi]^T$. Since the speed and state of HOV are defined in two different coordinate systems, it is necessary to obtain the relationship between the state in the inertial coordinate system and the speed in the body-fixed coordinate system. HOV coordinate system is shown in Fig. 2.

The kinematics equation of the HOV is as follows:

$$\dot{\eta} = J(\eta)v \quad (1)$$

where the coordinate transformation matrix is:

$$J(\eta) = \begin{bmatrix} J_1 & O_{3 \times 3} \\ O_{3 \times 3} & J_2 \end{bmatrix} \quad (2)$$

$$J_1(\eta) = \begin{bmatrix} \cos \psi \cos \theta & \cos \psi \sin \theta \sin \varphi - \sin \psi \cos \varphi \\ \sin \psi \sin \theta & \sin \psi \sin \theta \sin \varphi + \cos \psi \cos \varphi \\ -\sin \theta & \cos \theta \sin \varphi \end{bmatrix}, J_2(\eta) = \begin{bmatrix} 1 & \tan \theta \sin \varphi & \cos \varphi \tan \theta \\ 0 & \cos \varphi & -\sin \varphi \\ 0 & \sin \varphi / \cos \theta & \cos \varphi / \cos \theta \end{bmatrix}$$

$$\cos \psi \sin \theta \cos \varphi + \sin \psi \sin \varphi \\ \sin \psi \sin \theta \sin \varphi + \cos \psi \cos \varphi \\ \cos \theta \sin \varphi \end{bmatrix}$$

For the 4-DOF Deep-sea Warrior HOV $\varphi = 0$, $\theta = 0$, so, the kinematics equation of Deep-sea Warrior HOV is:

$$\dot{\eta} = \begin{bmatrix} \dot{x} \\ \dot{y} \\ \dot{z} \\ \dot{\psi} \end{bmatrix} = J(\eta)V = \begin{bmatrix} \cos \psi & -\sin \psi & 0 & 0 \\ \sin \psi & \cos \psi & 0 & 0 \\ 0 & 0 & 1 & 0 \\ 0 & 0 & 0 & 1 \end{bmatrix} \begin{bmatrix} u \\ v \\ w \\ r \end{bmatrix} \quad (3)$$

$$\dot{\tilde{\eta}} = \dot{\eta} - \dot{\eta}_d = \begin{bmatrix} 0 & 0 & 0 & -u_d \sin \psi_d - v_d \cos \psi_d \\ 0 & 0 & 0 & u_d \cos \psi_d - v_d \sin \psi_d \\ 0 & 0 & 0 & 0 \\ 0 & 0 & 0 & 0 \end{bmatrix} \begin{bmatrix} x - x_d \\ y - y_d \\ z - z_d \\ \psi - \psi_d \end{bmatrix} + \begin{bmatrix} \cos \psi_d & -\sin \psi_d & 0 & 0 \\ \sin \psi_d & \cos \psi_d & 0 & 0 \\ 0 & 0 & 1 & 0 \\ 0 & 0 & 0 & 1 \end{bmatrix} \begin{bmatrix} u - u_d \\ v - v_d \\ w - w_d \\ r - r_d \end{bmatrix} \quad (8)$$

2.2. QPSO-MPC-based kinematics controller

2.2.1. HOV linear error model

Obviously, all sampling points on the reference trajectory are applicable to kinematics equation. For the dth reference trajectory point, the kinematics equation without ocean current is:

$$\dot{\eta}_d = J(\eta_d)v_a \quad (4)$$

where $\eta_d = [x_d \ y_d \ z_d \ \psi_d]^T$, $v_a = [u_d' \ v_d' \ w_d' \ r_d']^T$. It is assumed that the 4-DOF ocean current speed in the inertial coordinate system is $v_o = [u_x \ v_y \ w_z \ 0]^T$, the ocean current value can be obtained by the following transformation:

$$\begin{cases} u_u = u_x \cos \psi_d + v_y \sin \psi_d \\ v_v = -u_x \sin \psi_d + v_y \cos \psi_d \\ w_w = w_z \end{cases} \quad (5)$$

where u_u , v_v , w_w are the ocean current at surge, sway, and heave. The expected relative speed at dth point is:

$$u_d = u_d' - u_u, v_d = v_d' - v_v, w_d = w_d' - w_w, r_d = r_d' \quad (6)$$

So, the reference speed in ocean current is $v_d = [u \ v \ w \ r]^T$, by applying Taylor series expansion formula (4), ignoring the second-order and above part of the Taylor expansion term at the reference point, it can be expressed as follows:

$$\begin{aligned} \dot{\eta} &= J(\eta_d)v_d + \left. \frac{\partial J(\eta)v}{\partial \eta} \right|_{\eta=\eta_d} (\eta - \eta_d) \\ &\quad v = v_d \\ &+ \left. \frac{\partial J(\eta)v}{\partial v} \right|_{\eta=\eta_d} (v - v_d) \\ &\quad v = v_d \end{aligned} \quad (7)$$

It is worth noting that, although what HOV kinematics modeling

obtains is a nonlinear system. But for MPC, the requirement of model accuracy is low and there is an iterative optimization process. It is especially suitable for the HOV system which has the characteristics of model uncertain and slow speed. So, the linear error model is fully applicable.

The HOV liner error model can be calculated by subtracting (4) from (7):

The HOV linear error model used to design MPC controller, which must be discretized. By discretizing formula (8), the following formula can be obtained:

$$\tilde{\eta}(k+1) = A_{k,t}\tilde{\eta}(k) + B_{k,t}\tilde{v}(k) \quad (9)$$

2.2.2. Prediction model

In the objective function, it is essential to calculate the future system output in predictive domain. The following change is made to formula (9):

$$\xi(k|t) = \begin{bmatrix} \tilde{\eta}(k|t) \\ \tilde{v}(k-1|t) \end{bmatrix} \quad (10)$$

Then, the new state space will be represented as:

$$\xi(k+1|t) = \tilde{A}_{k,t}\xi(k|t) + \tilde{B}_{k,t}\Delta v(k|t) \quad (11)$$

$$\gamma(k|t) = \tilde{C}_{k,t}\xi(k|t) \quad (12)$$

After deductions, the predicted system output could be got as follows:

$$Y(t) = \Psi_t\xi(t|t) + \Theta_t\Delta V(t) \quad (13)$$

2.2.3. QPSO rolling optimization

The deviation between control system state and reference system state and control quantity are added to the objective function to ensure the MPC tracking effect is ideal. The designed objective function is as follows:

$$\begin{aligned} F(k) &= \sum_{i=1}^{N_p} \|\eta(k+i|t) - \eta_d(k+i|t)\|_Q^2 \\ &+ \sum_{i=1}^{N_c-1} \|\Delta V(k+i|t)\|_R^2 + \rho\varepsilon^2 \end{aligned} \quad (14)$$

In addition, in the actual control system, the following system constraints must be met:

Control constraint:

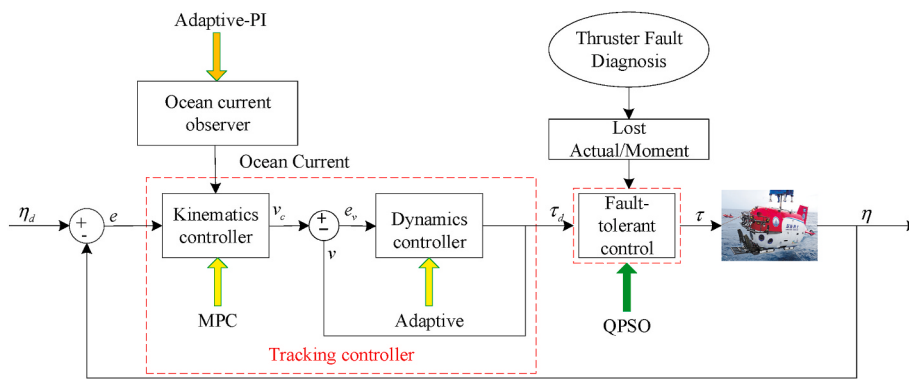


Fig. 3. The cascaded dynamic tracking controller for thruster fault.

$$v_{\min}(t+k) \leq v(t+k) \leq v_{\max}(t+k) \quad k=0, 1, \dots, N_c - 1$$

Control increment constraint:

$$\Delta v_{\min}(t+k) \leq \Delta v(t+k) \leq \Delta v_{\max}(t+k) \quad k=0, 1, \dots, N_c - 1$$

The stability constraints are expressed as follows:

$$\|\eta(k+N_p|t) - \eta_d(k+N_p|t)\|_Q^2 = 0$$

The complete form of the objective function is:

$$F(\xi(t), v(t-1), \Delta V(t)) = \Delta V(t) H_t \Delta V(t)^T + G_t \Delta V(t)^T \quad (18)$$

Therefore, in every step, solving optimization problems under the constraints of MPC is equivalent to solve quadratic programming problems:

$$\begin{aligned} & \min_{\Delta V(t)} \Delta V(t) H_t \Delta V(t)^T + G_t \Delta V(t)^T \\ \text{s.t. } & V_{\min} \leq \Delta V_t + V_t \leq V_{\max} \\ & \Delta V_{\min} \leq \Delta V_t \leq \Delta V_{\max} \end{aligned} \quad (19)$$

2.2.4. Feedback mechanism

The QPSO optimization process seen as section 2.2.3. Until $t = \text{MAXITER}$, the whole optimization process is over. Then, the global optimal position is back to the HOV control system as the control input. After the QPSO optimization process, a series of control increments are obtained:

$$\Delta V_{c_t}^* = [\Delta v_{c_t}^* \quad \Delta v_{c_{t+1}}^* \quad \dots \quad \Delta v_{c_{t+N_c-1}}^*]^T \quad (20)$$

According to the principle of MPC, the first element of the control sequence is applied to the system to complete the tracking control at this time:

$$v_c(t) = v_c(t-1) + \Delta v_{c_t}^* \quad (21)$$

2.3. Dynamics modeling

The HOV system movement control is primarily related to gravity, buoyancy, thrust, hydrodynamic force, interference force and multi-various moments relevant to these forces. Under the action of these forces and moments, the nonlinear dynamics equation of HOV under 6-DOF is as following:

$$M\ddot{v} + C(v)v + D(v)v + g(\eta) = \tau \quad (22)$$

In this paper assumed the body-fixed coordinate system origin coincides with the center of gravity of the HOV. The inertial matrix of HOV is:

(15)

(16)

(17)

$$M_{RB} = \begin{bmatrix} m & 0 & 0 & 0 & 0 & 0 \\ 0 & m & 0 & 0 & 0 & 0 \\ 0 & 0 & m & 0 & 0 & 0 \\ 0 & 0 & 0 & I_x & -I_{xy} & -I_{xz} \\ 0 & 0 & 0 & -I_{yx} & I_y & -I_{zy} \\ 0 & 0 & 0 & -I_{zx} & -I_{zy} & I_z \end{bmatrix} \quad (23)$$

The hydrodynamic additional inertial matrix as:

$$M_A = - \begin{bmatrix} X_{\dot{u}} & X_{\dot{v}} & X_{\dot{w}} & X_{\dot{p}} & X_{\dot{q}} & X_{\dot{r}} \\ Y_{\dot{u}} & Y_{\dot{v}} & Y_{\dot{w}} & Y_{\dot{p}} & Y_{\dot{q}} & Y_{\dot{r}} \\ Z_{\dot{u}} & Z_{\dot{v}} & Z_{\dot{w}} & Z_{\dot{p}} & Z_{\dot{q}} & Z_{\dot{r}} \\ K_{\dot{u}} & K_{\dot{v}} & K_{\dot{w}} & K_{\dot{p}} & K_{\dot{q}} & K_{\dot{r}} \\ M_{\dot{u}} & M_{\dot{v}} & M_{\dot{w}} & M_{\dot{p}} & M_{\dot{q}} & M_{\dot{r}} \\ N_{\dot{u}} & N_{\dot{v}} & N_{\dot{w}} & N_{\dot{p}} & N_{\dot{q}} & N_{\dot{r}} \end{bmatrix} \quad (24)$$

In consideration of the speed of HOV in the water is relatively slow, in this paper, the centripetal force and Coriolis matrix C will be ignored. Hydrodynamic damping matrix can be divided into friction resistance matrix D_L and viscous pressure resistance matrix D_Q .

$$D(v)v = D_L v + D_Q \text{diag}(|v|)v \quad (25)$$

Gravity and buoyancy term $g(\eta)$ also be ignored in this paper because the HOV is designed as “zero” buoyancy through counterweight, that is, gravity is equal to buoyancy. For the 4-DOF Deep-sea Warrior HOV, the simplify dynamics model is:

$$\left\{ \begin{array}{l} \tau_X = m(\dot{u} - vr) - 0.5\rho L^3(X'_{vr}vr + LX'_{rr}r^2) \\ \quad - 0.5\rho L^2(X'_{uu}u^2 + X'_{vv}v^2 + X'_{ww}w^2 + X'_{uw}uw) \\ \tau_Y = m(\dot{v} + ur) - 0.5\rho L^3Y'_rur \\ \quad - 0.5\rho L^2[Y'_vuv + Y'_{vw}vw + Y'_{wv}wv] \left((v^2 + w^2)^{1/2} \right) \\ \tau_Z = -0.5\rho L^2[Z'_wuw + Z'_{|w|}u|w| + Z'_{ww}w(w^2 + v^2)^{1/2}] \\ \quad + Z'_{vw}v^2 + Z'_{|v|w}|v|w + Z'_{w|w|}w \left((v^2 + w^2)^{1/2} \right) \\ \quad - 0.5\rho L^3Z'_{vr}vr + mw \\ \tau_N = I_z\dot{r} - 0.5\rho L^3[N'_vuv + N'_{|v|v}|v| \left((v^2 + w^2)^{1/2} \right) \\ \quad + N'_{vw}vw] - 0.5\rho L^5N'_{r|r|r}|r| \\ \quad - 0.5\rho L^4[N'_rur + N'_{|v|r}|v| \left((v^2 + w^2)^{1/2} \right) |r|] \end{array} \right. \quad (26)$$

2.4. Adaptive-based dynamics controller

HOVs, typical strongly coupled nonlinear system, are hard to finish the trajectory tracking control by the traditional linear control method. At the same time, the external complex hydrodynamic parameters are

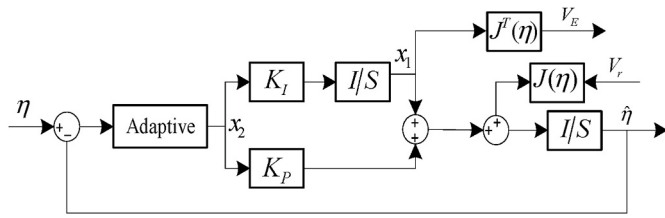


Fig. 4. Ocean current observer with adaptive-PI method.

hard to compute, and the HOV movement always change with time. Not to mention the interference exist in the actual ocean current environment. Therefore, it is unrealistic to establish an exact dynamics model, so most model-based control methods are also hard to control HOV track tracking accurately. The adaptive mechanism adopts the change of speed error to modify controller parameters. Therefore, the thrust output from the dynamics controller changes accordingly, thereby reducing the position error. After considering the ocean current interference, the goal of the dynamics controller is to make the movement speed v_r of HOV relative to the ocean current to track the reference relative speed v_c . The actual position of the HOV in the inertial coordinate system is obtained by solving the following equation:

$$\dot{\eta} = J(\eta)(v_r + v_b) \quad (27)$$

Where, $v = v_r + v_b$ is the actual tracking speed of HOV, define the virtual speed error as:

$$e_c = v_c - v \quad (28)$$

The sliding mode surface constructed by the speed error is:

$$s = \dot{e}_c + 2\Lambda e_c + \Lambda^2 \int e_c \quad (29)$$

The adaptive dynamic control law is:

$$\tau = \Phi(\dot{v}_r, v_r, v, \eta) \hat{\theta} - K_d s \quad (30)$$

Assuming that $\dot{\theta} = 0$, the adaptive law of parameter $\hat{\theta}$ is:

$$\dot{\hat{\theta}} = -\Gamma \Phi^T(\dot{v}_r, v_r, v, \eta) s \quad (31)$$

The cascaded dynamic tracking controller for thruster fault is in Fig. 3.

2.5. Ocean current observer design

The speed synthesis method needs to combine the actual ocean current speed and the actual HOV speed then introduce into it to kinematic controller. But in a marine environment, there is time-varying ocean current and its size cannot be accurately measured.

In this section, an ocean current observer is devised to predict the ocean current v_E when the ocean current is unknown. The proportional-integral (PI) control is used to design the ocean current observer (Alonge et al., 2001). In this paper, the adaptive algorithm is used to optimize the parameters of PI control, because adaptive algorithm can enable the controller to modify itself characteristics to suit to the dynamic characteristics of target and disturbance, which can improve the performance of PI control and deal with time-varying ocean current more effectively. The adaptive-PI ocean current observer is shown in Fig. 4.

The closed-loop state space model is as follows:

$$\begin{cases} \dot{x}_1 = K_I x_2 \\ \dot{x}_2 = -x_1 - K_P x_2 + \dot{\eta}_E \end{cases} \quad (32)$$

Where $x_2 = \eta - \hat{\eta}$ express the position evaluated error. $\hat{\eta}$ is the evaluated of position η . $\dot{\eta}_E = J(\eta)^* v_E$ denotes the ocean current speed in the

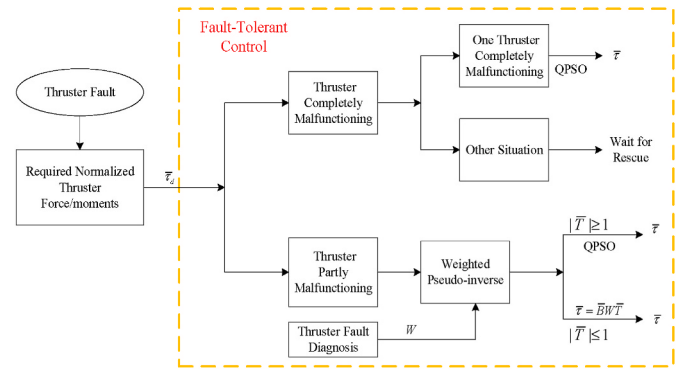


Fig. 5. The block diagram of thruster fault-tolerant control.

inertial coordinate system. The PI control parameters are $K_I = 1$ and $K_P = 1$.

2.6. The time-varying ocean current

In order to simulate the actual time-varying ocean current situation encountered by HOV during underwater mission, the time-varying current probability model is designed through the following rules in this paper:

The HYCOM-based simulation results of the mouth of the Hangzhou Bay are showed in (Chen et al., 2015). And the traditional circulation distribution of western Guangdong, Qiongzhou Strait and Beibu Gulf in summer are showed in (Yang et al., 2003). We can also get the current speed in most of China's coastal water is between 0 m/s-0.5 m/s, and the probability of 0.2 m/s-0.5 m/s is about 35%. The proportion of sea area higher than 0.5 m/s is about 5% (Guo, 2013).

3. Thruster fault-tolerant control

In this section, the case of thruster failure is introduced into the trajectory tracking process. In this work, the fault information is assumed to have been determined by some known fault diagnosis methods. The main work of this paper is to propose a fault-tolerant control method based on QPSO and weighted pseudo inverse method to produce the required HOV thruster force/moment. The fault-tolerant control block diagram of deep-sea warrior HOV thrusters are shown in Fig. 5. It should be noted that the control strategy can be applied to different types of HOVs in a similar manner.

3.1. Hybrid thruster reconfiguration strategy

Fault-free thruster normalized thrust formula is:

$$\bar{\tau} = \bar{B}^* \bar{T} \quad (33)$$

The Deep-sea Warrior HOV normalization fault-free thruster configuration matrix (Omerdic and Roberts, 2004) is:

$$\bar{B} = \begin{bmatrix} 0.5 & 0.5 & 0 & 0 & 0 & 0 \\ 0 & 0 & 0 & 0 & 1 & 0 \\ 0 & 0 & 0.3333 & 0.3333 & 0 & 0.3333 \\ 0 & 0 & 0.1191 & 0.1191 & 0.3047 & -0.4571 \\ -0.113 & 0.113 & 0.1701 & 0.1701 & 0 & 0.4338 \\ 0.2193 & 0.2193 & 0 & 0 & 0.5613 & 0 \end{bmatrix}$$

As shown in Fig. 5, the hybrid thruster reconfiguration method for thruster fault-tolerant control in this paper can be described as follows. First, the actual normalization control signals $\bar{\tau}$ are computed by weighted pseudo-inverse method, then produce the normalization thruster force \bar{T} (the calculation formula in two cases is shown in Fig. 5). If all normalized thruster force/moment are in the range of saturation point $-1 \leq \bar{T} \leq 1$, this solution is used directly in next process. If any

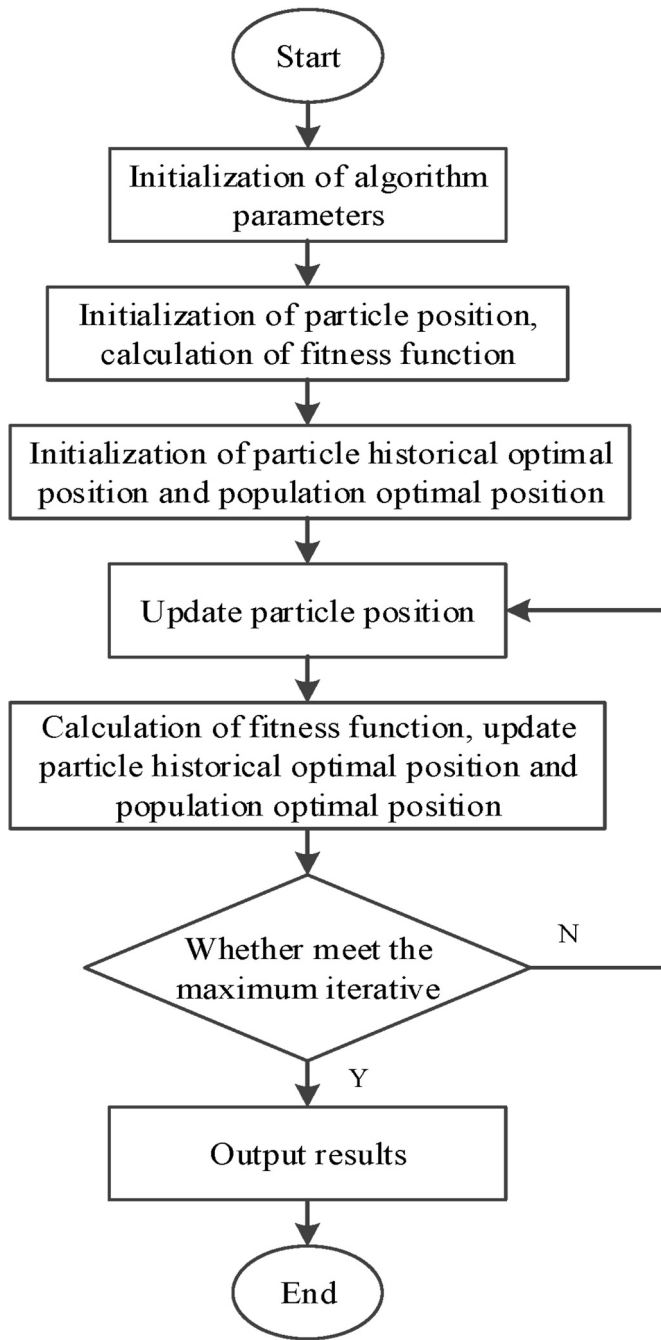


Fig. 6. The flow chart of QPSO.

normalized thruster force/moment are out of the saturation range, QPSO algorithm should be applied in order to redistribute between normal running thrusters to obtain the required normalization thruster force.

3.2. Thruster completely malfunctioning

When a thruster is completely damaged (such as the i th thruster), delete the corresponding column of normalization thruster configuration matrix \bar{B} , and then \bar{B} converts to a 6×5 matrix \bar{B}_i . The solution space is not unique at this time. At this moment, the best solution can be obtained through the QPSO optimization method which details are in section 3.3.2. It is very rare that more than one thruster fails completely during the mission. The best method is to wait for rescue.

3.3. Thruster partly malfunctioning

3.3.1. Weighted pseudo-inverse method

When thruster partly damaged, normalization thruster force/moment can be calculated by the degree of thruster failure which express by a diagonal weighting matrix. The diagonal weighting matrix can be defined as:

$$W = \text{diag}(w_1 \ w_2 \ w_3 \ w_4 \ w_5 \ w_6) \in R^{6 \times 6}$$

$$w_i = \begin{cases} 0 < w_i \leq 1, & \text{if the } i\text{th thruster is in partly failure, } i = 1 \sim 6 \\ 1, & \text{if the } i\text{th thruster is not in failure} \end{cases} \quad (34)$$

Weighting coefficient w_i is the degree of thruster failure. The bigger the w_i , the smaller the fault and vice versa.

3.3.2. QPSO algorithm

In QPSO model, the state of particles is described by wave function rather than position and speed. The dynamic behavior of particles is different from the particles in traditional particle swarm optimization (PSO) algorithm, because the exact values x and V cannot be determined at the same time. The objective function is defined by the l_∞ norm of the thruster force. The l_∞ norm of the thruster force manifold $\bar{T} = [\bar{T}_1 \ \bar{T}_2 \ \bar{T}_3 \ \bar{T}_4 \ \bar{T}_5 \ \bar{T}_6]$ is defined as:

$$\|\bar{T}\|_\infty = \max\{|\bar{T}_1|, |\bar{T}_2|, |\bar{T}_3|, |\bar{T}_4|, |\bar{T}_5|, |\bar{T}_6|\} \quad (35)$$

For equation $\bar{\tau} = \bar{B}\bar{W}\bar{T}$, it can be written as:

$$\begin{aligned} \bar{\tau}_X &= w_1\bar{T}_1 + w_2\bar{T}_2 \\ \bar{\tau}_Y &= w_5\bar{T}_5 \\ \bar{\tau}_Z &= w_3\bar{T}_3 + w_4\bar{T}_4 + w_6\bar{T}_6 \\ \bar{\tau}_K &= 0.93w_3\bar{T}_3 + 0.93w_4\bar{T}_4 + 2.38w_5\bar{T}_5 - 3.57w_6\bar{T}_6 \\ \bar{\tau}_M &= -0.93w_1\bar{T}_1 + 0.93w_2\bar{T}_2 + 1.4w_3\bar{T}_3 + 1.4w_4\bar{T}_4 + 3.57w_6\bar{T}_6 \\ \bar{\tau}_N &= 0.93w_1\bar{T}_1 + 0.93w_2\bar{T}_2 + 2.38w_5\bar{T}_5 \end{aligned} \quad (36)$$

One inverse function can be given as:

$$\begin{aligned} \bar{T}_1 &= \bar{\tau}_1 \\ \bar{T}_2 &= (\bar{\tau}_X - w_1\bar{\tau}_1)/w_2 \\ \bar{T}_3 &= (1.4\bar{\tau}_Z - \bar{\tau}_M - 1.86w_1\bar{\tau}_1 + 0.93\bar{\tau}_X)/4.34w_3 \\ \bar{T}_4 &= (1.4\bar{\tau}_Z - \bar{\tau}_M - 1.86w_1\bar{\tau}_1 + 0.93\bar{\tau}_X)/4.34w_4 \\ \bar{T}_5 &= \bar{\tau}_Y/w_5 \\ \bar{T}_6 &= (1.4\bar{\tau}_Z - \bar{\tau}_M - 1.86w_1\bar{\tau}_1 + 0.93\bar{\tau}_X)/(-2.17w_6) \end{aligned} \quad (37)$$

Where $w_2, w_3, w_4, w_5, w_6 \neq 0$. Finally, using equation (37), the amount of calculation is reduced by simplifying the optimization problem into a single parameter adjustment problem under the objective criterion equation (35), and the most appropriate control force is selected in the solution space. After thruster normalization, $[-1, 1]$ are the thrust saturation limits, so the constrained optimization problem becomes to acquire the smallest l_∞ norm thrust value as the feasible solution. The formula expression is as follows:

$$\text{minimize} \|\bar{T}\|_\infty, \text{ subject to } \bar{\tau} = \bar{B}\bar{W}\bar{T}, -1 \leq \bar{T}_i \leq 1, i = 1 \sim 6 \quad (38)$$

The flow chart of QPSO is shown in Fig. 6. It should be noted that l_∞ norm thrust allocation is not energy minimization but a solution to minimize all the thruster forces in the solution space, so that the HOV can have more maneuvering ability.

4. Simulation and discussion

To test the proposed algorithm, simulation study was conducted on Deep-sea Warrior HOV. In this section, the simulation results of proposed method which joint QPSO-MPC-based kinematics controller, adaptive-based dynamics controller and fault-tolerant control will be shown.

Table 1

The control parameters for QPSO-MPC.

N_p	N_c	Λ	k	Γ	K
10	10	1	1	1	100

In this section, the thruster fault information is set to $W = \text{diag}(0.6 \ 0.6 \ 1 \ 1 \ 1)$ (1HT, 2HT thrust loss is 40% of normal thrust). Simulation sampling time T is 0.1s.

The detailed data of the Deep-sea Warrior HOV is: Mass in air is $m = 20$ ton, the device is 9.3 m in length, 3 m in width and 4 m in height.

And the hydrodynamic parameters are:

$$\left\{ \begin{array}{l} X'_u = -21.12, \ X'_{uu} = -31.17, \ X'_{vv} = 3.44, \ X'_{ww} = 27.39 \\ X'_{rr} = 9.267, \ X'_{uw} = 8.06, \ X'_{vr} = 13.56, \ Y'_{v} = -132.206 \\ Y'_{r} = 1.827, \ Y'_{v} = -251.81, \ Y'_{r} = 1.827, \ Y'_{v|v|} = -306.12 \\ Y'_{v|r|} = -137.78, \ Y'_{r|r|} = 1.25, \ Y'_{vw} = 263.41, \ Z'_{w} = -116.125 \\ Z'_{w} = -101.67, \ Z'_{|w|} = 37.25, \ Z'_{w|w|} = -337, \ Z'_{ww} = -116.17 \\ Z'_{vv} = -38.04, \ Z'_{rr} = -55.75, \ Z'_{vr} = 93.37, \ Z'_{|v|w} = 73.93 \\ N'_{v} = 1.827, \ N'_{r} = -4.916, \ N'_{v} = -65.04, \ N'_{r} = -39.94 \\ N'_{v|v|} = 31.72, \ N'_{|v|r} = -97.93, \ N'_{r|r|} = -6.699, \ N'_{vw} = -18.606 \end{array} \right.$$

4.1. Polygonal line tracking in the ocean current

For the proposed Deep-sea Warrior HOV, the expected speed of the selected reference trajectory can fully meet the speed and driving constraints. The given trajectory and initial speed presented as:

When $0 \leq t < 50$ s:

$$\left\{ \begin{array}{l} x_d(t) = 0 \\ y_d(t) = 0 \\ z_d(t) = 0.3*t \\ \psi_d(t) = 0 \end{array} \right. , \quad \left\{ \begin{array}{l} u_d(t) = 0m/s \\ v_d(t) = 0m/s \\ w_d(t) = 0.3m/s \\ r_d(t) = 0rad/s \end{array} \right.$$

When $50s \leq t < 100s$:

$$\left\{ \begin{array}{l} x_d(t) = 0.3*(t - 50) \\ y_d(t) = 0 \\ z_d(t) = 15 \\ \psi_d(t) = 0 \end{array} \right. , \quad \left\{ \begin{array}{l} u_d(t) = 0.3m/s \\ v_d(t) = 0m/s \\ w_d(t) = 0m/s \\ r_d(t) = 0rad/s \end{array} \right.$$

When $100s \leq t < 150s$:

$$\left\{ \begin{array}{l} x_d(t) = 15 \\ y_d(t) = 0.3*(t - 50) \\ z_d(t) = 15 \\ \psi_d(t) = \pi/2 \end{array} \right. , \quad \left\{ \begin{array}{l} u_d(t) = 0m/s \\ v_d(t) = 0.3m/s \\ w_d(t) = 0m/s \\ r_d(t) = 0rad/s \end{array} \right.$$

When $150s \leq t < 200s$:

$$\left\{ \begin{array}{l} x_d(t) = 15 - 0.3*(t - 50) \\ y_d(t) = 15 \\ z_d(t) = 15 \\ \psi_d(t) = \pi \end{array} \right. , \quad \left\{ \begin{array}{l} u_d(t) = -0.3m/s \\ v_d(t) = 0m/s \\ w_d(t) = 0m/s \\ r_d(t) = 0rad/s \end{array} \right.$$

The parameter settings of traditional adaptive control are $\Gamma = 1, k_d = 25,000, \Lambda = 1$. The QPSO-MPC control parameters are listed in Table 1. In addition, both the population size (popsize) and the MAXITER are set as 50.

The control process in ocean current after thruster fault is as follows: e is the error of the actual trajectory after thruster fault and the reference trajectory, then it is applied to the kinematics controller. Meanwhile, combined with the speed synthesis method, the ocean current was incorporated into the kinematics controller to eliminate the influence of unknown current. The kinematics controller transmits the speed error between expected speed and actual speed to dynamics controller, then

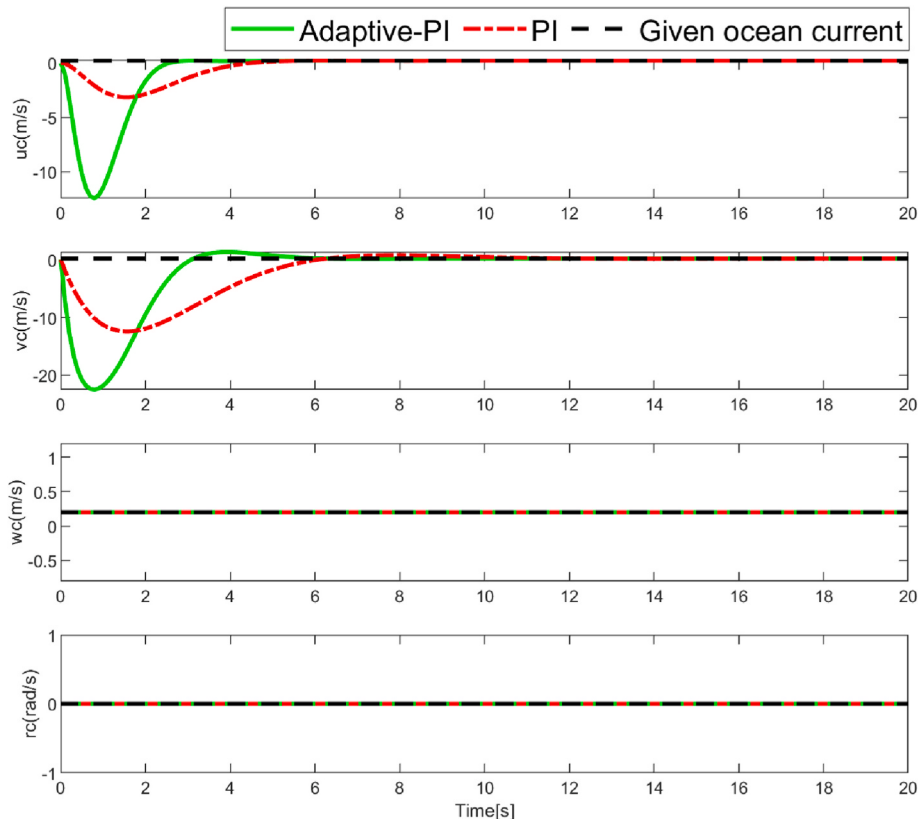


Fig. 7. Adaptive-PI ocean current observer.

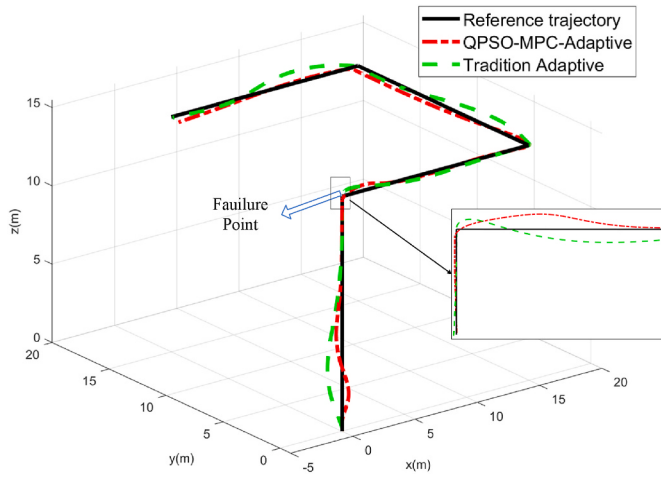


Fig. 8. Comparison of three-dimension polygonal line tracking.

dynamics controller passes $\bar{\tau}_d$ on fault-tolerant control. Based on proposed fault-tolerant control, redistribute force/moment between normal running thrusters to obtain $\bar{\tau}$. Next, apply $\bar{\tau}$ to HOV. By constantly adjusting, finally, making the error e gradually converge to zero.

The polygonal line ocean current estimation situation can be obtained by the Adaptive-PI ocean current observer which is shown in Fig. 7. PI control has overshoot and can stably estimate the current speed in the seventh second, while Adaptive-PI can achieve stable estimation in only 5 s without overshoot. The results show that the adaptive-PI can estimate the unknown ocean current speed quickly and stably.

4.2. Comparison of trajectory tracking effects with traditional adaptive and NMPC

In this part, the tracking effects under thruster fault of QPSO-MPC adaptive method, traditional adaptive algorithm, nonlinear-MPC (NMPC) are given respectively for Deep-sea Warrior HOV, and the tracking performance in constant ocean current is compared and analyzed to verify that the speed constraint ability of QPSO-MPC adaptive method can solve driving saturation problem which caused by speed jump when thruster failure.

The simulation information of polygonal line trajectory tracking is as follows. Simulation time is 200s. The constant current is $v_o = [0.2 \ 0.2 \ 0.2 \ 0]^T$.

The given trajectory and initial speed for polygonal line can be consulted in section 4.1.

Fig. 8 is a comparison of the tracking effect between the QPSO-MPC adaptive method and traditional adaptive algorithm. Due to the continuous action of three-dimensional ocean current, the tracking trajectory controlled by traditional adaptive algorithm deviates from the given trajectory, and is accompanied by oscillation adjustment process. QPSO-MPC adaptive method has better tracking effect, more stable tracking and smaller tracking error.

In Fig. 9 and Fig. 10, the black dotted line respectively represents the maximal and minimal values of speed or normalized thrust. In the simulation process, in order to more obviously reflect the effect of fault-tolerant, the thruster fault point is set at $t = 50$ s which is placed together with the polygonal line break point.

Though the formula $M\dot{v} + C(v)v + D(v)v + g(\eta) = \tau$, fault information $W = \text{diag}(0.6 \ 0.6 \ 1 \ 1 \ 1 \ 1)$ and the maximal and minimal values of speed, we can get the maximal and minimal values of speed under the fault information.

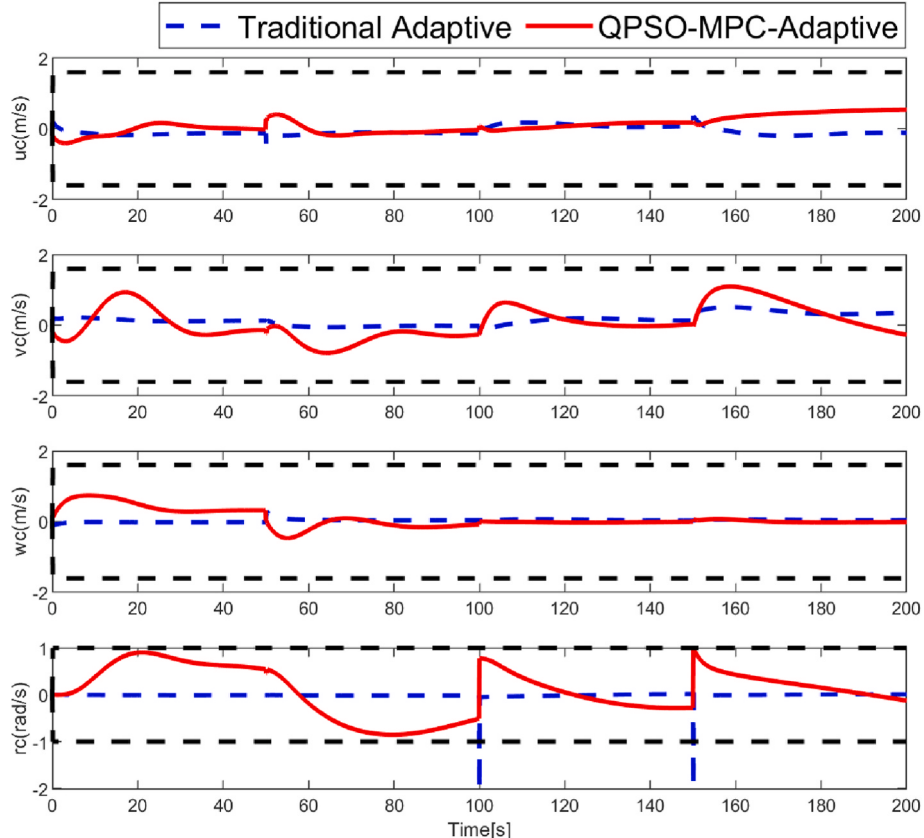


Fig. 9. Speed change in the tracking process.

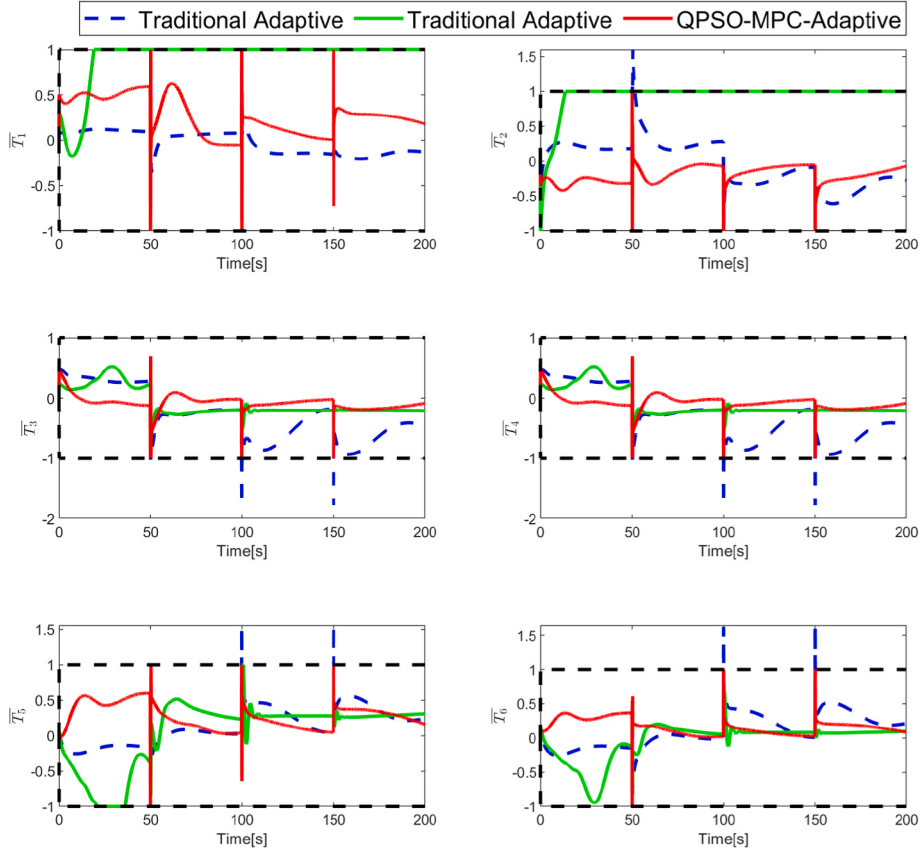


Fig. 10. Normalized thrust variation.

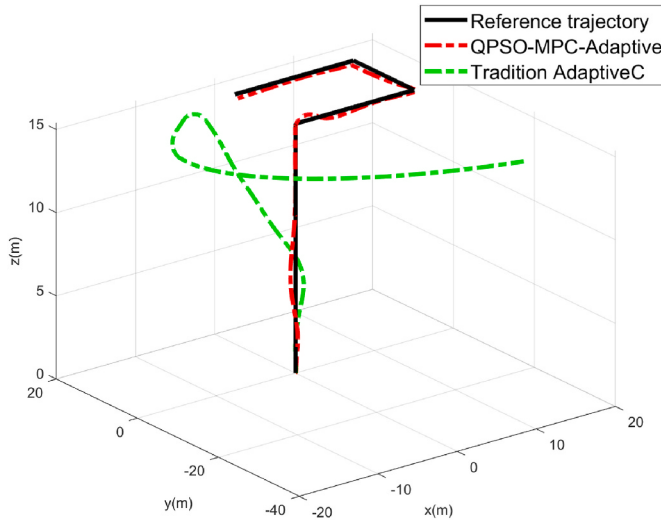


Fig. 11. Comparison of three-dimension polygonal line tracking.

$$\begin{aligned}
 -1.6\text{m/s} &\leq u(t+k) \leq 1.6\text{m/s} & k = 0, 1, \dots, N_c - 1 \\
 -1.6\text{m/s} &\leq v(t+k) \leq 1.6\text{m/s} & k = 0, 1, \dots, N_c - 1 \\
 -2\text{m/s} &\leq w(t+k) \leq 2\text{m/s} & k = 0, 1, \dots, N_c - 1 \\
 -1\text{m/rad} &\leq r(t+k) \leq 1\text{m/rad} & k = 0, 1, \dots, N_c - 1
 \end{aligned}$$

Speed comparison of QPSO-MPC adaptive method and traditional adaptive algorithm is shown in Fig. 9. For the traditional adaptive algorithm, because there is positive correlation between the control law and large state error, so, lead to speed jump phenomenon. For example, r_i is changed toward -2 m/rad when HOV thruster faults. This is beyond the minimal speed -1 m/rad of HOV. It means that the excessive speed

change will produce in short time by using traditional adaptive algorithm. This leads to the existence of too large acceleration, which needs the thrust big enough. It is very obvious beyond the maximal thrust limit under thruster failure.

As shown in Fig. 10, normalized thrusts of traditional adaptive algorithm cannot meet the constraint $-1 \leq \bar{T}_i \leq 1$, $i = 1, 2, 3, 4, 5, 6$. $\bar{T}_1, \bar{T}_2, \bar{T}_3, \bar{T}_4, \bar{T}_5, \bar{T}_6$ generated by traditional adaptive algorithm are over the range. For instance, the maximal normalized thrust \bar{T}_2 is even as far as 8.97.

To limit traditional adaptive algorithm thrust overrun problem, the normalized thrusts of traditional adaptive algorithm with thrust constraint can be applied in Fig. 10.

The track effect of traditional adaptive algorithm with thrust constraint in Fig. 11. Obviously, if the thrust of the traditional adaptive algorithm is limited within the thrust limit, it is impossible to use this algorithm to achieve trajectory tracking. It is evident from Figs. 9 and 10 that the QPSO-MPC adaptive method limits the speed and normalized thrust in the extent of range, which means that the speed jump problem of the traditional adaptive algorithm in the case of thruster failure is perfectly solved.

The error comparison of trajectory tracking of QPSO-MPC adaptive method, traditional adaptive algorithm, and traditional adaptive algorithm with thrust constraint in Fig. 12. It further proves the track tracking effect of QPSO-MPC adaptive method is better than other controllers.

Fig. 13 is the comparison of the track tracking effect between QPSO-MPC adaptive method and NMPC algorithm. NMPC algorithm constructs a dynamic control law through position and attitude error information, which only considers thrust constraints, but does not consider speed changes. For QPSO-MPC adaptive method, the dynamic control law is designed by using the deviation between the virtual desired speed which is designed based on the position error and the

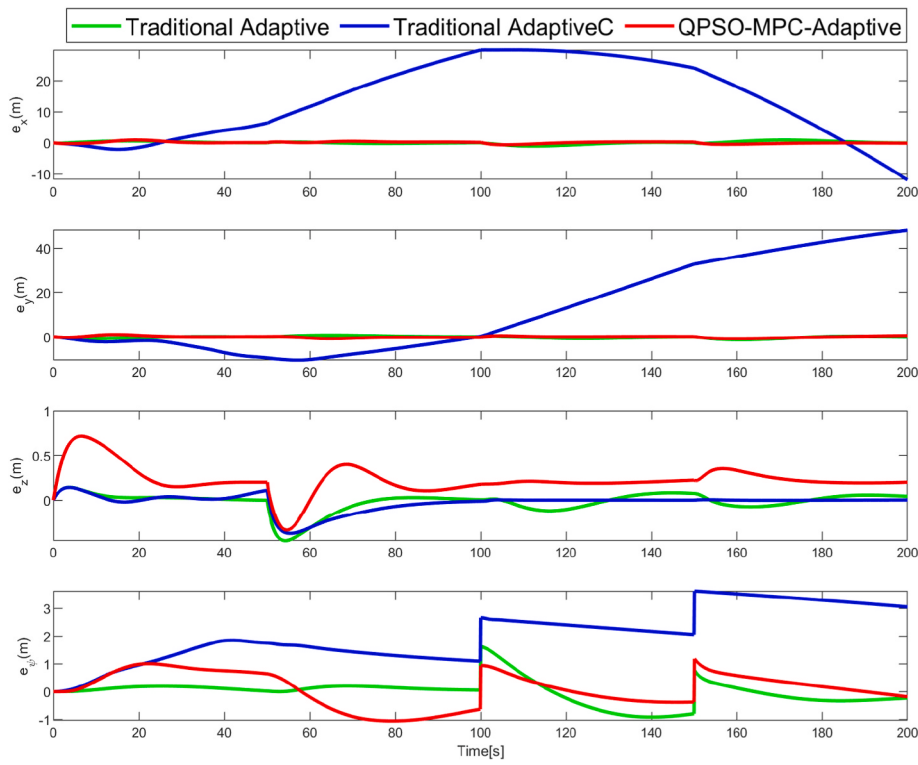


Fig. 12. Trajectory tracking error.

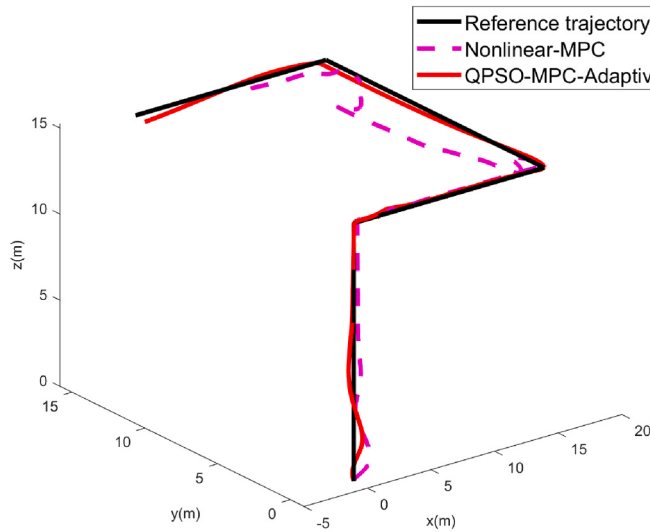


Fig. 13. Comparison of three-dimension polygonal line tracking.

actual speed. It can be seen that under the influence of constant ocean current, the control effect deviation of NMPC algorithm is large and the tracking effect is poor from the initial stage.

In a word, the application of QPSO-MPC adaptive method can overcome the problem of driving saturation and realize stable trajectory tracking with thruster fault.

4.3. Fault-tolerant control comparison with pseudo inverse method

In this section, taking the Deep-sea Warrior HOV in section 4.2 as a particle, it can satisfy speed and drive control signals. The simulation information of polygonal line trajectory tracking is the same as section 4.1, 4.2. The trajectory tracking simulation results and the simulation

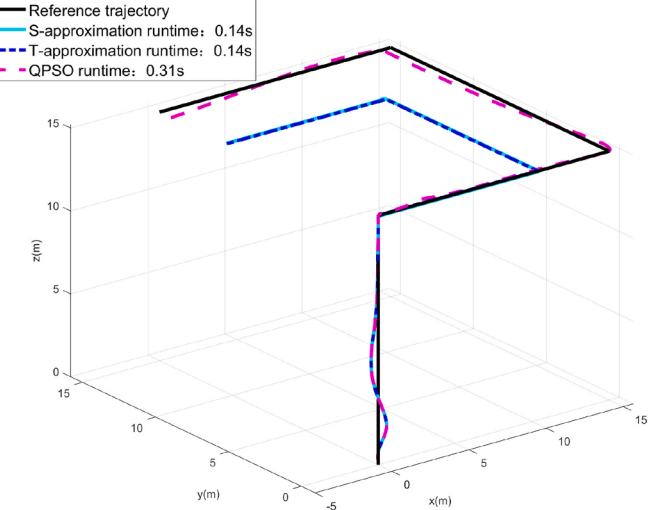


Fig. 14. Comparison of polygonal line tracking effect.

time to find a suitable solution of fault-tolerant control based on QPSO and pseudo inverse method (S-approximate and T-approximate) are shown in Fig. 14. There are four segments of the polygonal line proposed in this section, the normalized thrust in the second segments ($50s < t \leq 100s$) is $\bar{T} = [0.6863 \ 0.1660 \ -0.4 \ -0.4 \ -0.1528 \ 0.9926]$. By formula $\bar{\tau} = \bar{B}^* \bar{T}$, the normalized thrust without fault is $\bar{\tau} = [0.4261 \ -0.1528 \ 0.0642 \ -0.5955 \ 0.2357 \ 0.1011]$. After thruster fault, we can get the weighted pseudo inverse solution in the case of failure is:

$$\bar{T} = [1.1438 \ -0.5451 \ -0.1515 \ -0.1515 \ 0.2767 \ 0.3400]$$

The normalized reconstruction thrust produced by S-approximation, T-approximation and QPSO is as follows:

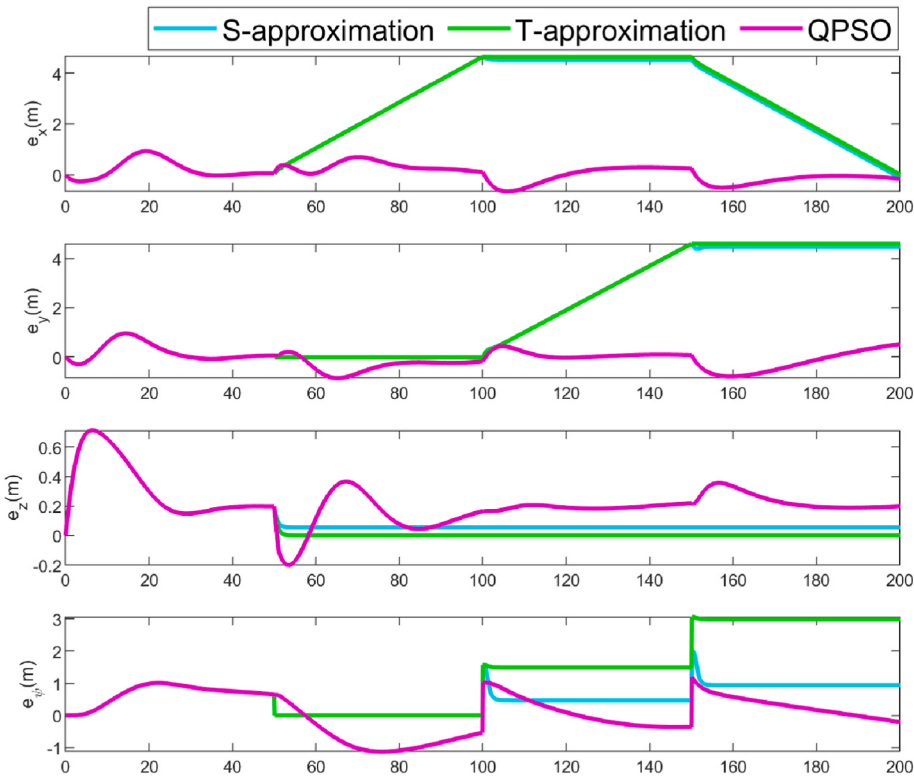


Fig. 15. Trajectory tracking error.

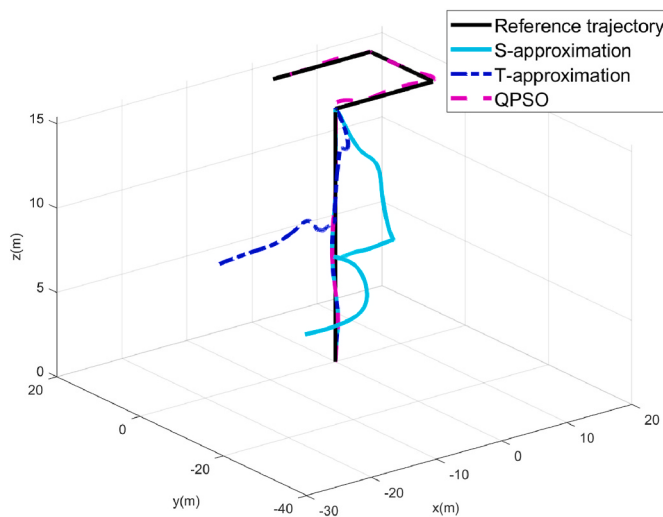


Fig. 16. Comparison of polygonal line tracking effect.

$$\bar{T}_S = [1 \ -0.5451 \ -0.1515 \ -0.1515 \ 0.2767 \ 0.3400]$$

$$\bar{T}_T = [1 \ -0.4766 \ -0.1325 \ -0.1325 \ 0.2419 \ 0.2973]$$

$$\bar{T}_{QPSO} = [0.9338 \ -0.6685 \ -0.6310 \ 0.3502 \ 0.2767 \ 0.3177]$$

As can be seen from Fig. 14, the time required for QPSO and weighted pseudo inverse methods to find a suitable solution is 0.31s and 0.14s. In terms of time, it is acceptable. But, because the weighted pseudo inverse solution is out of range, the errors of the magnitude and direction which cause by scaling or truncation exist and the HOV cannot follow the desired trajectory completely.

Meanwhile normalized thrust produced by QPSO algorithm is fully

meet the requirements. We can obtain the error contrast of trajectory tracking of in Fig. 15, QPSO delay (tracking error after stabilization) approaching zero. The pseudo inverse method has a lager delay obvious.

Based on the polygonal line simulation tracking results above, it can be confirmed that QPSO-MPC adaptive method can realize stable trajectory tracking and effective thrust distribution in constant ocean current. Different from the constant ocean current, the size of time-varying current cannot be accurately measured and change over time, which requires higher performance of control algorithm. The time-varying ocean current model is shown in section 2.5.

The trajectory tracking simulation results of fault-tolerant control based on QPSO and pseudo inverse method (S-approximate and T-approximate) in time-varying ocean current are shown in Fig. 16. We can obtain the error contrast of trajectory tracking in Fig. 17. In the time-varying current environment, there are more and disordered normalized weighted pseudo inverse solutions are beyond the range of solutions after thruster failure. But the QPSO fault-tolerant simulation results are good as the results of constant ocean current.

Obviously, the proposed trajectory tracking controller with fault-tolerant control can come true stable trajectory tracking control compared with pseudo inverse fault-tolerant method.

4.4. Robustness analysis

When operating at different underwater environment, the external forces of HOV will be changed. A certain anti-interference ability should be considered in the proposed method.

In order to test the anti-interference ability of the proposed method for external disturbances uncertainty, in this section, three different external disturbances of 5%, 10% and 20% are added to the thrust calculation. The polygonal line simulation case is employed to verify QPSO-MPC adaptive method tracking performance with thruster fault when existing external disturbances (for parameters setting, refer to section 4.1, 4.2). In order to more obviously reflect the effect of fault-tolerant, the thruster failure point is also set at $t = 50$ s. The fault

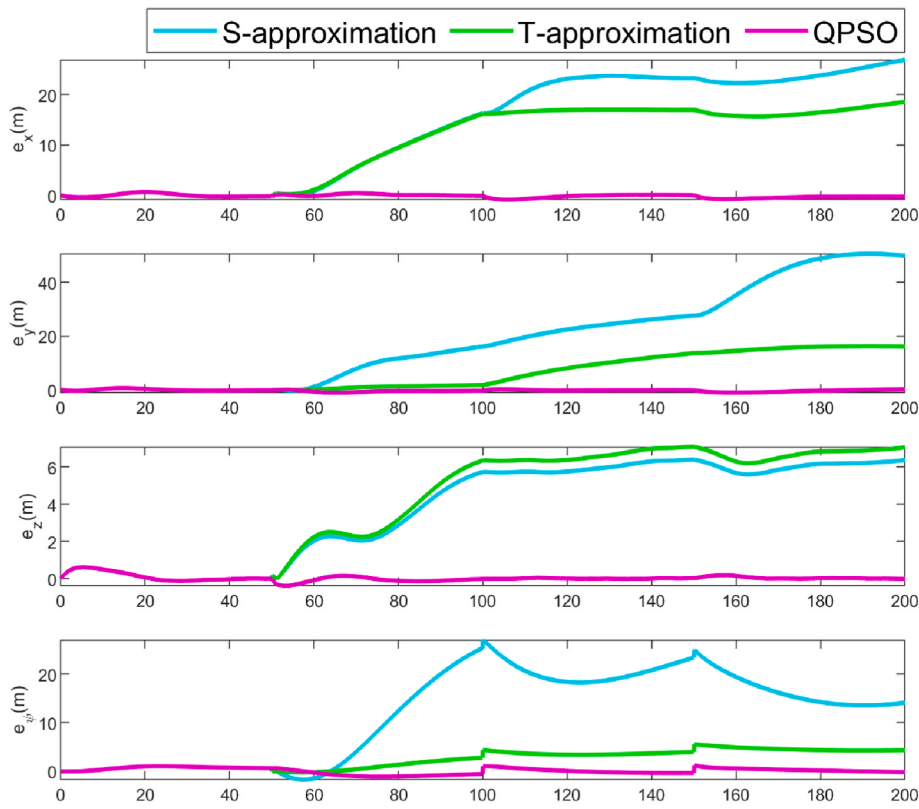


Fig. 17. Trajectory tracking error.

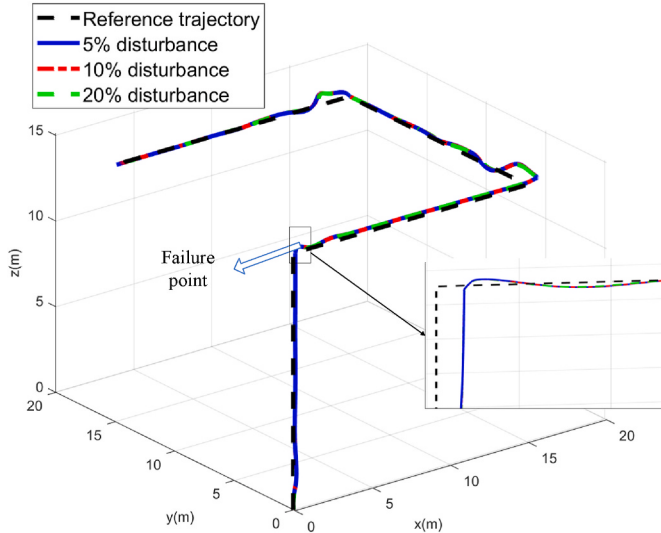


Fig. 18. Polygonal line tracking with uncertainty external forces in constant ocean current.

point and the break point are put together. The dynamic trajectory tracking simulation results of QPSO-MPC adaptive method under different conditions are showed in Fig. 18 and Fig. 19. It can be clearly seen that under different external interference uncertainties, at the situation of constant ocean current, the tracking stabilizes quickly after thruster failure, and the tracking error is very small, which can be basically ignored. Although, in the time-varying ocean current environment, there is a certain error at the beginning, at the end, the reference trajectory is reached.

Therefore, it can be considered that the proposed dynamic trajectory

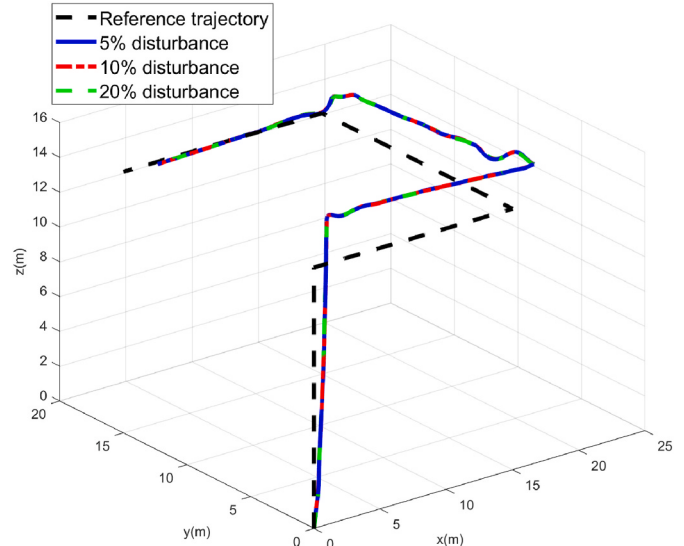


Fig. 19. Polygonal line tracking with uncertainty external forces in time-varying ocean current.

tracking controller with thruster fault-tolerant control has strong robustness, can overcome the problem of external interference and achieve stable tracking.

5. Conclusion

This paper studies the trajectory tracking problem of HOV with thruster failure in ocean current. First, the method of thruster fault-tolerant control based on QPSO is investigated for HOV. Second, MPC

is employed to realize solution to the speed jump problem. Considering the computational burden for nonlinear HOV dynamics models, the MPC method is used in conjunction with adaptive control to achieve dynamic tracking control, which solves problems of modeling uncertainty and external disturbances. Combined with the speed synthesis method, the influence of ocean current was incorporated into the design of kinematics control law. Meanwhile, the observer based on Adaptive-PI control is designed to estimate the unknown ocean current. The simulation results verified the effectiveness of the dynamic trajectory tracking controller with thruster fault-tolerant control in the complex ocean current environment.

CRediT authorship contribution statement

Huapeng Zhang: Methodology, Software, Validation, Writing – original draft, Writing – review & editing, Visualization. **Daqi Zhu:** Conceptualization, Methodology, Supervision, Project administration, Funding acquisition. **Chenxia Liu:** Supervision. **Hu Zhen:** Supervision.

Declaration of competing interest

The authors declare that they have no known competing financial interests or personal relationships that could have appeared to influence the work reported in this paper.

Acknowledgements

This research is supported by the National Natural Science Foundation of China (62033009, U1706224), Shanghai Science and Technology Innovation Funds (206510712300).

References

- Alonge, F., D' Lppolito, F., Raimondi, F.M., 2001. Trajectory Tracking of Underactuated Underwater Vehicles. Proceedings of the 40th IEEE Conference on Decision and Control (Cat. No.01CH37228), pp. 4421–4426. Orlando, FL, USA.
- Benosman, M., Lum, K., 2009. Online references reshaping and control reallocation for nonlinear fault-tolerant control. *IEEE Trans. Control Syst. Technol.* 17 (2), 366–379.
- Chen, X.B., Zhou, L., Chen, X., 2015. Comparative study on vertical coordinates of HYCOM model in East China Sea. *Mar. Sci.* 39 (7), 60–68.
- Cho, S.J., Zhang, F.M., Edwards, C.R., 2017. Adaptive learning for controlled Lagrangian particle tracking. *OCEANS 2016 MTS/IEEE Monterey* 1–6.
- Fabiani, F., Grechi, S., Tommasina, S.D., Caiti, A., 2016. A NLPCA Hybrid Approach for AUV Thrusters Fault Detection and Isolation. 2016 3rd Conference on Control and Fault-Tolerant Systems..
- Fossen, T.I., Sagatun, S.I., 1991. Adaptive control of nonlinear underwater robotics systems. Proceedings. 1991 IEEE International Conference on Robotics and Automation 12 (2), 95–105.
- Gan, W.Y., Zhu, D.Q., Hu, Z., 2020a. A model predictive adaptive control algorithm for human occupied vehicle. *IEEE Trans. Ind. Electron.* 67 (9), 7829–7839.
- Gan, W.Y., Zhu, D.Q., Hu, Z., Shi, X.P., Yang, L., Chen, Y.S., 2020b. Model predictive adaptive constraint tracking control for underwater vehicles. *IEEE Trans. Ind. Electron.* 67 (9), 7829–7840.
- Gao, J., Proctor, A.A., Shi, Y., Bradley, C., 2016. Hierarchical model predictive image-based visual servoing of underwater vehicles with adaptive neural network dynamic control. *IEEE Trans. Cybern.* 46 (10), 2323–2334.
- Guo, Y.Q., 2013. Mathematical Modeling and Observation Results Analysis of Vertical Motion of Submarine Buoy in the South China Sea Land Slope Bottom Current Observation. Shandong, First Institute of Oceanography, State Oceanic Administration.
- Han, P.H., Li, G.Y., Skulstad, R., Skjøng, S., 2020. A deep learning approach to detect and isolate thruster failures for dynamically positioned vessels using motion data. *IEEE Trans. Instrum. Meas.* 70, 1–11.
- Li, X., Zhu, D.Q., 2018. An adaptive SOM neural network method to distributed formation control of a group of AUVs. *IEEE Trans. Ind. Electron.* 65 (10), 8260–8270.
- McCue, L., 2016. Handbook of marine craft hydrodynamics and motion control bookshelf. *IEEE Control Syst. Mag.* 36 (1), 78–79.
- Naeem, W., Sutton, R., Chudley, J., 2004. Model predictive control of an autonomous underwater vehicle with a fuzzy objective function optimized using a GA. IFAC Proceedings Volumes 37 (10), 433–438.
- Omerdic, E., Roberts, G., 2004. Thruster fault diagnosis and accommodation for open-frame underwater vehicles. *Control Eng. Pract.* 12 (12), 1575–1598.
- Peng, Z.H., Wang, J., Han, Q.L., 2019. Path-following control of autonomous underwater vehicles subject to velocity and input constraints via neurodynamic optimization. *IEEE Trans. Ind. Electron.* 66 (11), 8724–8732.
- Shen, C., Buckingham, B., Shi, Y., 2017. Modified C/GMRES algorithm for fast nonlinear model predictive tracking control of AUVs. *IEEE Trans. Control Syst. Technol.* 25 (5), 1896–1904.
- Shen, C., Shi, Y., Buckingham, B., 2018. Trajectory tracking control of an autonomous underwater vehicle using Lyapunov-based model predictive control. *IEEE Trans. Ind. Electron.* 65 (7), 5796–5805.
- Soylu, S., Buckingham, B.J., Podhorodeski, R.P., 2008. A chattering-free sliding-mode controller for underwater vehicles with fault-tolerant infinity-norm thrust allocation. *Ocean Eng.* 35 (16), 1647–1659.
- Sun, J., Xu, W.B., Feng, B., 2004. A global search strategy of quantum-behaved particle swarm optimization. *Singapore IEEE Conference on Cybernetics and Intelligent Systems* 1, 111–116.
- Valdes, A., Khorasani, K., 2010. A pulsed plasma thruster fault detection and isolation strategy for formation flying of satellites. *Appl. Soft Comput.* 10 (3), 746–758.
- Wang, Y.J., Zhang, M.J., Wilson, P.A., 2015. Adaptive neural network-based backstepping fault tolerant control for underwater vehicles with thruster fault. *Ocean Eng.* 110 (1), 15–24.
- Yan, Z.P., Deng, C., Zhou, J.J., Zhao, Y.F., 2012. Research on Dive Plane Trajectory Tracking Control Method of AUV under Current Disturbance. Proceedings of the 10th World Congress on Intelligent Control and Automation, pp. 3887–3891.
- Yan, Z.P., Yu, H.M., Zhang, W., 2015. Globally finite-time stable tracking control of underactuated UUVs. *Ocean Eng.* 107 (1), 132–146.
- Yang, S.Y., Bao, X.W., Chen, C.S., 2003. Characteristics and production mechanism of coastal current in western Guangdong in summer. *Acta Oceanographica Sinica* 25 (6), 1–8.
- Zhang, Y.M., Jiang, J., 2008. Bibliographical review on reconfigurable fault-tolerant control systems. *Annu. Rev. Control* 32 (2), 229–252.
- Zhu, D.Q., Liu, Q., Hu, Z., 2011. Fault-tolerant control algorithm of the manned submarine with multithruster based on quantum-behaved particle swarm optimization. *Int. J. Control.* 84 (11), 1817–1829.